Journal of Alloys and Compounds 507 (2010) 419–424

Contents lists available at ScienceDirect

Journal of Alloys and Compounds

journal homepage: www.elsevier.com/locate/jallcom

Wettability and interfacial reactions between the molten Sn–3.0 wt%Ag–0.5 wt%Cu solder (SAC305) and Ni–Co alloys

Yue-ting Chen, Ya-ting Chan, Chih-chi Chen*

R&D Center for Membrane Technology and Department of Chemical Engineering, Chung Yuan Christian University, #200, Chung Pei Rd., Chung Li, 320 Taiwan

ARTICLE INFO

Article history:
Received 12 May 2010
Received in revised form 31 July 2010
Accepted 4 August 2010
Available online 11 August 2010

Keywords:
Intermetallics
Liquid–solid reactions
Diffusion
Phase diagrams

ABSTRACT

This study examines the wetting properties and interfacial reactions between molten Sn–3.0 wt%Ag–0.5 wt%Cu solder and Ni–Co alloys to evaluate Ni–Co alloys as alternative diffusion barrier layer materials in flip chip packaging for Cu/low k integrated circuits. The wetting properties of Ni–Co alloys with Sn–3.0 wt%Ag–0.5 wt%Cu solder are better than the currently used Ni–7 wt%V. With increased Co, the surface roughness of Ni–Co alloys increase and the wetting properties decrease. The Co effects on Sn–3.0 wt%Ag–0.5 wt%Cu/Ni–Co interfacial reactions are verified. The Sn–Ni–Co isothermal section illustrates the reaction paths. As Co increases from 10 to 40 at%, the reaction path shifts from the Sn–Ni side towards the Sn–Co side. The reaction rates in the different reaction couples are determined. The Ni–10 at%Co has the lowest reaction rate with the Sn–3.0 wt%Ag–0.5 wt%Cu solder.

© 2010 Elsevier B.V. All rights reserved.

1. Introduction

Because of smaller packaging size, greater I/O flexibility, and higher operating frequency, flip chip packaging maintains high interest [1,2]. Flip chip packaging requires under bump metallurgy (UBM) [3–6]. Of all the UBM layers, the diffusion barrier layer is the most important. Ni-based alloys, such as sputtering Ni–V [3,4] and electroplated/electroless Ni–P [5,6] are the commonly used diffusion barrier layers of UBM. As the integrated circuits move from Al to Cu metallization, UBM materials need to be re-evaluated [7]. Ni–Co alloys are good diffusion barriers for Cu up to 500 °C [8], and Co is another diffusion barrier layer material of UBM [9–13]. Ni–Co alloys are potential materials as an alternative diffusion barrier layer in flip chip packaging for Cu/low k integrated circuits.

This study examines the wetting properties and interfacial reactions between Ni–Co alloys and the Sn–3.0 wt%Ag–0.5 wt%Cu solder to evaluate the Ni–Co alloys as alternative diffusion barrier layer materials. In the reflow step, the molten solder contacts the substrate, wets the substrate, causing an interfacial reaction and forming soldering joints. Wetting properties and interfacial reactions affect soldering joints. Eutectic and near eutectic Sn–Ag–Cu solders are promising lead free solders [14–18]. Past research explores the wetting properties [5,6,18–31] and interfacial reactions [14–18] between Sn–Ag–Cu solders and various substrates, but not for Sn–Ag–Cu/Ni–Co systems. In this study, the Wilhelmy type wetting balance method determines the wetting properties [32]. Ni–Co alloys with 10, 20, and 40 at%Co additions are examined to verify the Co effect on the wetting properties and interfacial reactions. A relative phase diagram illustrates the reaction paths of different Co additions.

2. Experimental method

Ni–Co alloys were prepared with pure Ni wire (99.95 wt%, Aldrich Sigma, USA) and Co shots (99.95 wt%, Aldrich Sigma, USA) in an induction furnace. The solder used was the commercial Sn–3.0 wt%Ag–0.5 wt%Cu (SAC305, Shenmao Tech. Inc., Taoyuan, Taiwan). The solder ball size was 760 μm. A Wilhelmy wetting balance (SAT-5000, Rhesca, Tokyo, Japan) determined the wetting properties. Ni–Co substrates were cut into 10 mm × 5 mm × 1 mm. Before use, the Ni–Co substrates were lightly etched to remove the native oxide. The Ni–Co alloys were then fluxed and immersed into the solder bath. The solder bath was 250 °C. The immersion time, depth, and speed were 10 s, 4 mm, and 20 mm/s. The wetting time and wetting force were determined after each measurement. At least five measurements were conducted for each solder/Ni–Co system and the average data were reported.

Interfacial reactions were conducted using the reaction couple technique. A Ni–Co substrate was placed on a hot plate at 250 °C. A solder ball was then directly placed onto the Ni–Co substrate. Because 250 °C is higher than the melting point of the Sn–3.0 wt%Ag–0.5 wt%Cu solder, the solder ball melted, and the interfacial reaction occurred at the solder/substrate interface. For comparison, interfacial reactions between the same commercial

* Corresponding author. Tel.: +886 3 2654121; fax: +886 3 2654199.
E-mail addresses: ccchenj@cycu.edu.tw, ccchenj@gmail.com (C.-c. Chen).

0925-8388/$ – see front matter © 2010 Elsevier B.V. All rights reserved.
doi:10.1016/j.jallcom.2010.08.006

Sn–3.0 wt%Ag–0.5 wt%Cu solder and Ni were also examined. After finishing the predetermined reactions, the reaction couples were removed from the hot plate. The reaction couples were mounted and metallgraphically treated to reveal the interface. To make a better observation of the interface, some samples were partially etched with a 95%CH_3OH + 3%HNO_3 + 2%HCl (vol%) etchant. The etching time is 15 s. SEM (Scanning Electron Microscopy, Hitachi S-3000, Tokyo, Japan) equipped with BEI (Backscattered Electron Image) was used to observe the interface. EPMA (Electron Probe Microanalysis, JEOL, JXA-8200, Tokyo, Japan) with WDS (Wavelength Dispersive Spectroscopy) was used to determine the compositions of the reaction phases. The measurement precision was 100 ± 1 wt%. XRD (X-ray Diffraction, with Cu Kα1 radiation, BRUKE, D8A, Germany) was used for structural determinations. The thickness of the reaction phase was determined by dividing the area of the reaction phase by its linear length, conducted by a commercial software package. Thickness of at least 20 positions of the interface was measured and the average thicknesses were reported.

3. Results and discussion

Fig. 1 shows the wetting times and forces of the SAC305/Ni–Co systems. The wetting time represents the wetting rate; a shorter wetting time means a better wetting property. The wetting times of the SAC305/Ni–10 at%Co, SAC305/Ni–20 at%Co, and SAC305/Ni–40 at%Co systems are 0.89, 1.18, and 1.26 s. The determined wetting time of the SAC305/Ni system is 0.72 s, and the SAC305/Ni–7 wt%V is “non-wetting”. The wetting times of the SAC305/Ni–Co systems are longer than that of the SAC305/Ni system, and shorter than that of SAC305/Ni–7 wt%V. Using the wetting time as a wetting property indicator, the wetting property of Ni–Co alloys are better than Ni–7 wt%V, and poorer than the pure Ni. Co addition into the Ni substrate decreases the wetting property of Ni. The wetting times of the Ni–Co alloys are Ni–10 at%Co < Ni–20 at%Co < Ni–40 at%Co, indicating the wetting property of the Ni–Co alloys is Ni–10 at%Co > Ni–20 at%Co > Ni–40 at%Co. The wetting property of Ni–Co alloys decreases with Co additions. The wetting force shows nearly the opposite trend to the wetting time. A larger wetting force corresponds to a shorter wetting time, meaning a better wetting property. Because the wetting force depends on the perimeter of the substrate, the reported wetting forces normalize with the perimeter. The determined wetting forces of the SAC305/Ni–10 at%Co, SAC305/Ni–20 at%Co, and SAC305/Ni–40 at%Co systems are 0.236, 0.221, and 0.211 N/m, respectively. The determined wetting force

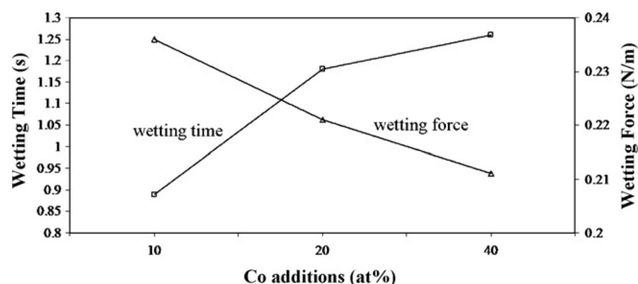

Fig. 1. Wetting times and forces of the SAC305/Ni–Co systems.

Fig. 2. Surface roughness of the substrates examined in this study. (a) Ni–10 at%Co, (b) Ni–20 at%Co, (c) Ni–40 at%Co and (d) surface roughness of the Ni–Co alloys.

of the SAC305/Ni system is 0.238 N/m, and the SAC305/Ni–7 wt%V system has no wetting force because it is "non-wetting". The wetting forces of the SAC305/Ni–Co systems are smaller than that of the SAC305/Ni. The wetting forces of the Ni–Co alloys are Ni–10 at%Co > Ni–20 at%Co > Ni–40 at%Co. Using the wetting force as a wetting property indicator, the wetting property of the Ni–Co alloys is Ni–10 at%Co > Ni–20 at%Co > Ni–40 at%Co. Using the wetting time and wetting force obtains the similar wetting results.

Fig. 2 shows the surface roughness of the Ni–Co substrates. The surface roughness of Ni–Co alloys ranges 100–600 nm. With increased Co, the surface roughness of the substrate increases. Ni–10 at%Co substrate is the smoothest, having the shortest wetting time and largest wetting force. Ni–40 at%Co substrate is the roughest, with the longest wetting time and smallest wetting force. The smoother substrate has better wetting properties. When the surface is rougher, the resistance for the molten solder to spray on the surface is greater, decreasing the wetting property. When the surface becomes smoother, the molten solder flows on the surface freely, increasing the wetting property. This result agrees with the prediction proposed by Shuttleworth and Bailey [33], and similar in solder/Ni–P and solder/Cu systems [5,6,18,20].

Besides the surface roughness, the driving force of wetting with molten solder on the substrate is the interfacial reaction [19]. Fig. 3(a) shows the BEI micrograph of the SAC305/Ni–10 at%Co couple reacted at 250 °C for 10 min. We observed only one reaction phase layer. Based on the EPMA compositional determination, its composition is Sn–0.1 at%Ag–10.0 at%Cu–28.8 at%Ni–2.7 at%Co. Co and Ni are chemically similar, and they can form a continuous solid solution except for the α–ε two-phase region [34]. Cu–Ni binary system is an isomorphous system [35]. Owing to the chemical similarity, Cu and Ni are with very extensive mutual solubility. Similar phenomena are also found in Sn–Ni–Cu [36,37] and Sn–Ni–Co [38] ternary systems. Because of the chemical similarity, Ni, Co, and Cu are identical in the intermetallic compounds. The (Cu + Ni + Co) content is 41.5 at%, and Sn is 58.4 at%. By referring to the Sn–Ni [39,40] and Sn–Co [41] binary phase diagrams, this phase is the Ni_3Sn_4 phase with 10.0 at%Cu, 2.7 at%Co, and negligible Ag solubility, or (Ni, Cu, Co)$_3$Sn$_4$. Ag does not actively participate in the interfacial reaction. The (Ni, Cu, Co)$_3$Sn$_4$ phase grows thicker with the longer reaction time. Fig. 3(b) shows the BEI micrograph of the SAC305/Ni couple reacted at 250 °C for 10 min. The composition of the reaction phase is Sn–0.1 at%Ag–7.0 at%Cu–35.0 at%Ni, which is the Ni_3Sn_4 phase with 7.0 at%Cu solubility. The Cu solubility in the Ni_3Sn_4 phase is 6.7 at% based on the Sn–Cu–Ni isothermal section at 240 °C [36]. The reaction phase of the SAC305/Ni–10 at%Co couple reacted at 250 °C is similar to that of SAC305/Ni. 10 at%Co addition does not alter the reaction path. The SAC305/Ni–10 at%Co interfacial reaction is also similar to that of Sn/Ni–10 at%Co. Fig. 3(c) shows the SEI micrograph of the Sn/Ni–10 at%Co couple reacted at 250 °C for 10 min. The reaction phase is also the Ni_3Sn_4 phase.

Fig. 4(a) displays the BEI micrograph of the SAC305/Ni–20 at%Co couple reacted at 250 °C for 10 min. For a better observation, the partial solder was etched away. We observe two reaction phases. The composition of the reaction phase adjacent to the Ni–20 at%Co substrate is Sn–0.4 at%Ag–0.4 at%Cu–23.5 at%Ni–9.9 at%Co. The content of (Cu + Ni + Co) is 33.8 at%, and Sn is 65.8 at%. By referring to the Sn–Ni–Co isothermal section at 250 °C [38] and Sn–Co binary phase diagram [41], this phase is the $CoSn_2$ phase with 23.5 at%Ni and negligible Cu and Ag solubility, or (Co, Ni, Cu)Sn$_2$. According to the composition, it appears to be the $NiSn_2$ phase with 9.9 at%Co solubility. However, based on the Sn–Ni binary phase diagram [39,40], the $NiSn_2$ phase does not exist in the Sn–Ni binary system. According to the Sn–Ni–Co phase equilibrium study [38], the $CoSn_2$ phase has relatively high Ni solubility, up to 25 at%. Therefore, this reaction phase is actually the $CoSn_2$ phase with considerate Ni solubility. Besides the $CoSn_2$ phase, another discontinuous phase forms between the solders and the $CoSn_2$ phase. The composition of this reaction phase is Sn–Sn–0.2 at%Ag–9.6 at%Cu–30.7 at%Ni–1.9 at%Co. It is the Ni_3Sn_4 phase with 9.6 at%Cu, 1.9 at%Co, and negligible Ag solubility. Because this Ni_3Sn_4 phase is not in a continuous layer type, it is from either the interfacial reaction or solidification precipitation during removal from the hot plate. Because the Ni solubility of the molten solder at 250 °C cannot form so much Ni_3Sn_4 phase, this Ni_3Sn_4 phase is not from the solidification precipitation, but from the solder/Ni–20 at%Co interfacial reactions. Therefore, the reaction phases of the SAC305/Ni–20 at%Co couple are the $CoSn_2$ and Ni_3Sn_4 phases. Fig. 4(b) illustrates the close-up of the interface of the SAC305/Ni–20 at%Co couple. X-ray diffraction verifies the reaction phases, as shown in Fig. 4(c). The total thickness of the reaction phases increases with the longer reaction time. The SAC305/Ni–20 at%Co interfacial reaction differs from those of SAC305/Ni–10 at%Co and SAC305/Ni. When the Co increases from 10 to 20 at%, it affects the interfacial reactions and forms the Sn–Co binary intermetallic compound, $CoSn_2$. The SAC305/Ni–20 at%Co

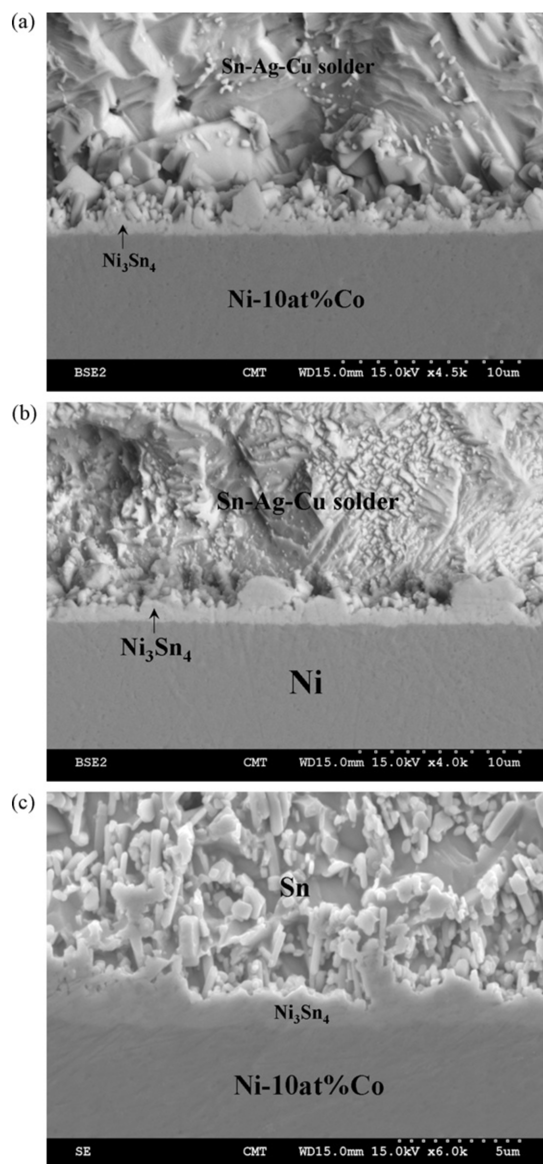

Fig. 3. (a) BEI micrograph of the SAC305/Ni–10 at%Co couple reacted at 250 °C for 10 min. (b) BEI micrograph of the SAC305/Ni couple reacted at 250 °C for 10 min. (c) SEI micrograph of the Sn/Ni–10 at%Co couples reacted at 250 °C for 10 min.

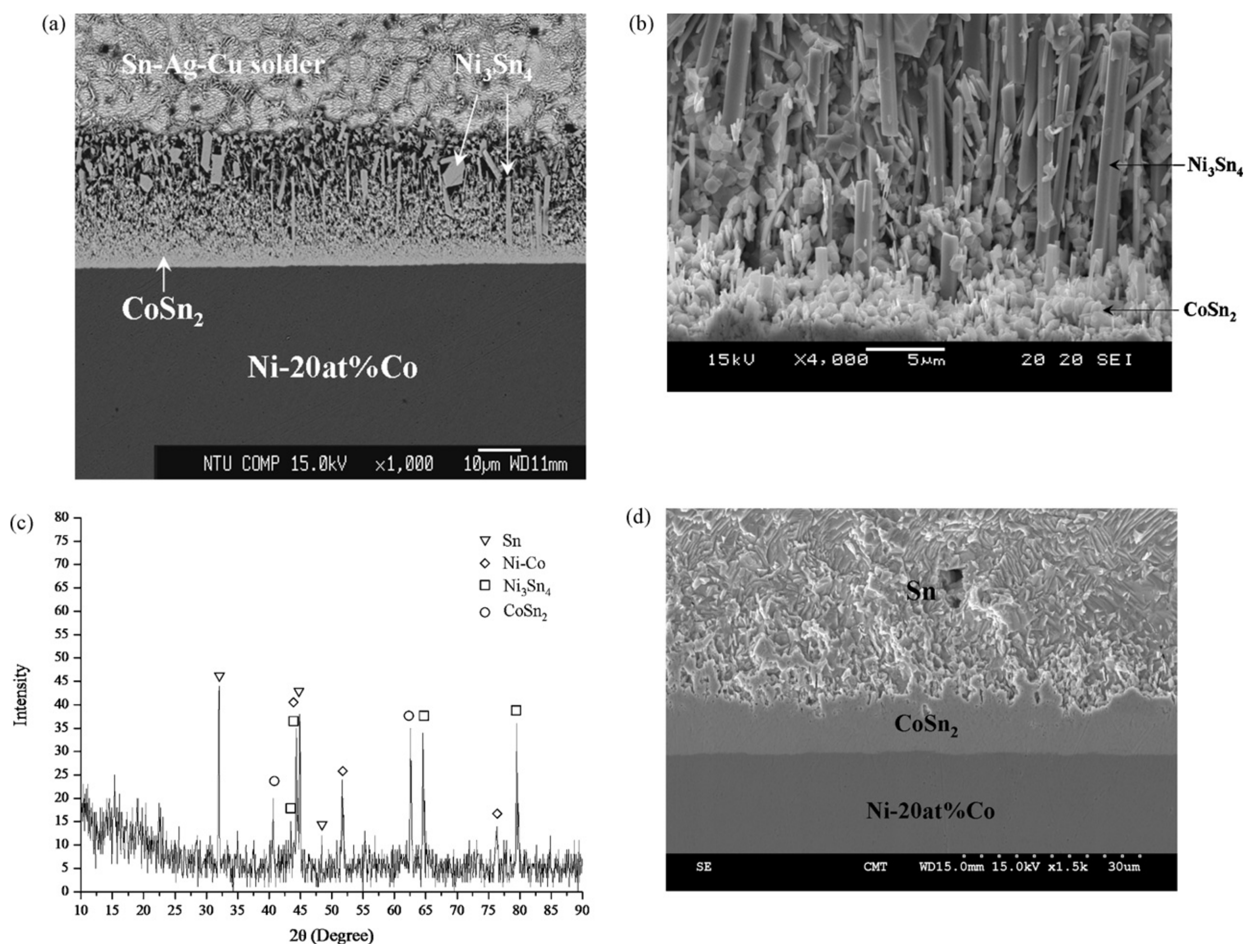

Fig. 4. The SAC305/Ni–20 at%Co couple reacted at 250 °C for 10 min (a) BEI micrograph, (b) close-up of the interface, (c) XRD pattern and (d) the Sn/Ni–20 at%Co couple reacted at 250 °C for 10 min.

interfacial reaction also differs from that of Sn/Ni–20 at%Co. Fig. 4(d) shows the SEI micrograph of the Sn/Ni–20 at%Co couple reacted at 250 °C for 10 min. The reaction phase is the $CoSn_2$ phase, which composition is Sn–22.3 at%Ni–10.4 at%Co. Comparing the SAC305/Ni–20 at%Co (Fig. 4(a)) and Sn/Ni–20 at%Co (Fig. 4(d)) interfacial reactions, the 0.5 wt%Cu enhances the formation of the (Ni, $Cu)_3Sn_4$ phase. The Sn/Ni–20 at%Co interfacial reaction at 250 °C shows a discrepancy in the literatures. Chao reported the reaction phase is the (Ni, Co)Sn_4 phase [38], while Takashi and Chen reported the reaction phase is the $CoSn_2$ phase [42,43].

Fig. 5(a) displays the SEI micrograph of the SAC305/Ni–40 at%Co couple reacted at 250 °C for 10 min. Careful examination reveals two reaction phases. The composition of the reaction phase adjacent to the Ni–40 at%Co substrate is Sn–0.1 at%Ag–0.8 at%Cu–16.7 at%Ni–15.7 at%Co, which is the $CoSn_2$ phase. The composition of the reaction phase between the solder and the $CoSn_2$ phase is Sn–1.8 at%Ag–3.1 at%Cu–8.7 at%Ni–11.4 at%Co. The Sn content is 75.0 at%, and (Cu + Ni + Co) is 23.2 at%. Referring to the Sn–Ni–Co isothermal section at 250 °C [38] and Sn–Co binary phase diagram [41], this reaction phase is the α-$CoSn_3$ phase with 8.7 at%Ni and 3.1 at%Cu solubility, or α-(Co, Ni, Cu)Sn_3. Accordingly, the reaction phases of the SAC305/Ni–40 at%Co couple are the α-$CoSn_3$ and $CoSn_2$ phases. Fig. 5(b) shows the close-up of the α-$CoSn_3$ phase, which exhibits a sheet-shaped grain. Fig. 5(c) displays the X-ray diffraction pattern of the SAC305/Ni–40 at%Co couple. The reaction phases grow thicker with the longer reaction time. When the Co addition is 40 at%, Co dominates the interfacial reaction. Only the Sn–Co intermetallic compounds, α-$CoSn_3$ and $CoSn_2$, are formed. The Sn–Ni intermetallic compound, Ni_3Sn_4, no longer exists. The SAC305/Ni–40 at%Co interfacial reaction differs from that of SAC305/Ni. Fig. 5(d) shows the SEI micrograph of the Sn/Ni–40 at%Co couple reacted at 250 °C for 10 min. The reaction phase is the α-$CoSn_3$ phase, which composition is Sn–11.9 at%Ni–12.5 at%Co. Chao examined Sn/Ni–40 at%Co interfacial reactions at 250 °C [38]. For 2 h, the reaction phase is the (Ni, $Co)_2Sn_7$ phase, which is not a thermodynamically stable phase. Comparing the SAC305/Ni–40 at%Co (Fig. 5(a)) and Sn/Ni–40 at%Co (Fig. 5(d)) interfacial reactions, the 0.5 wt%Cu enhances the formation of the $CoSn_2$ phase.

The Co effects on SAC305/Ni–Co interfacial reactions are verified. When the Co additions are 10, 20, and 40 at%, the reaction phases are the Ni_3Sn_4, Ni_3Sn_4/$CoSn_2$, and α-$CoSn_3$/$CoSn_2$ phases, respectively. A small amount of Cu or Co addition in solders can alter the reaction phases [44,45]. Cu and Co dominate kinetically. The observed interfacial reactions are results after competing between Cu and Co. For SAC305/Ni–10 at%Co couples, the Co effect is smaller than Cu. The SAC305/Ni–10 at%Co interfacial reaction is similar to SAC305/Ni. When the Co increases to 20 at%, the Co effect is comparable to that of Cu, forming the Cu-dissolved Ni_3Sn_4 and $CoSn_2$ phases. When the Co increases to 40 at%, the Co effect is larger than that of Cu. Co dominates the interfacial reactions, only forming Sn–Co intermetallics. The Sn–Ni–Co ternary phase diagram illustrates the reaction paths of SAC305/Ni–Co couples [38]. Fig. 6 shows the Sn–Ni–Co isothermal section at 250 °C superimposed with the reaction paths of the SAC305/Ni–Co couples. When the Co increases from 10 to 40 at%, the reaction path shifts from the Sn–Ni side towards the Sn–Co side. In SAC305/Ni–40 at%Co couples, the CoSn and Co_3Sn_2 phases are absent. Because the reaction kinetics

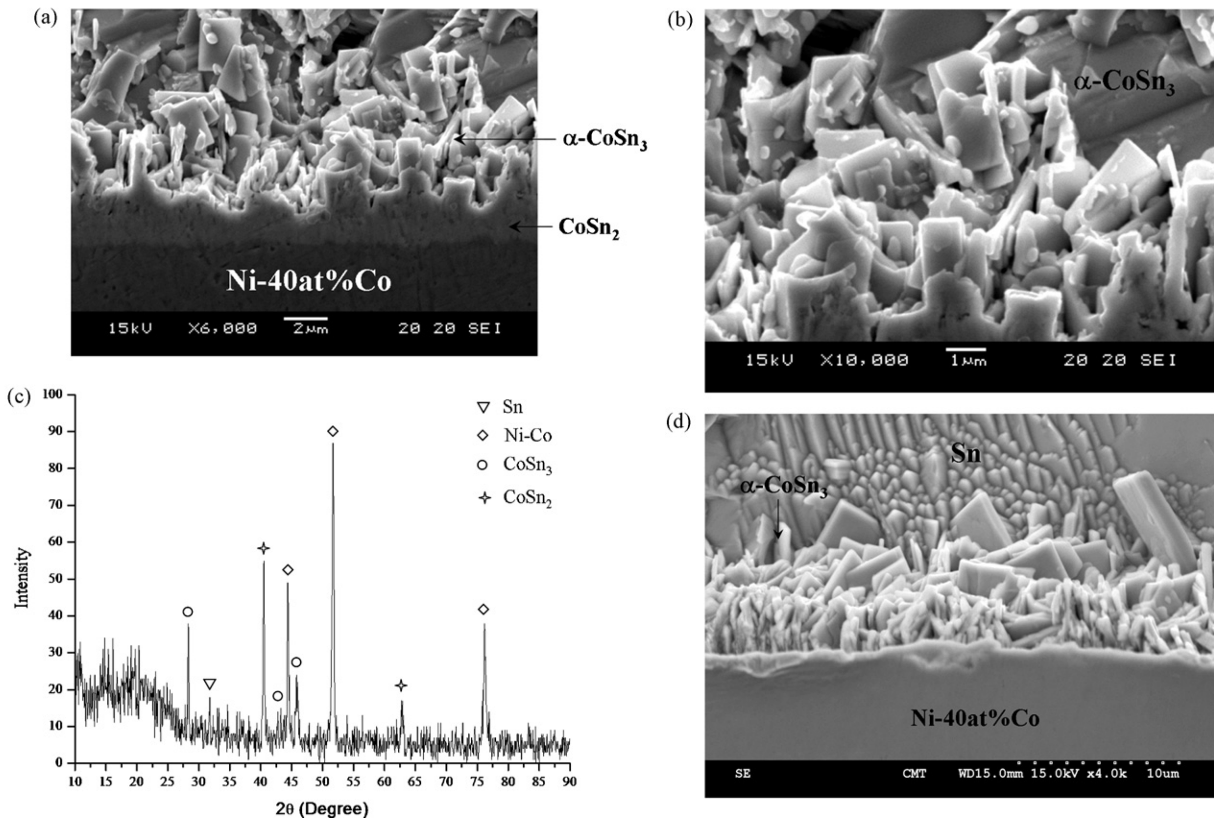

Fig. 5. The SAC305/Ni–40 at%Co reaction couple at 250 °C for 10 min. (a) SEI micrograph, (b) close-up of the α-$CoSn_3$ phase, (c) XRD pattern. (d) The Sn/Ni–40 at%Co couple reacted at 250 °C for 10 min.

dominate the interfacial reaction, some thermodynamically stable phases are not observed because of nucleation difficulty or being too thin to be observed [46,47].

Fig. 7 shows the total thickness of the reaction phases. The total thickness of the reaction phases is roughly linear dependent to square root of the reaction time, suggesting the interfacial reactions are diffusion controlled [48]. The slopes are the growth rate constants. Because the reaction phases differ in the three different reaction couples, their reaction rates also differ. The determined

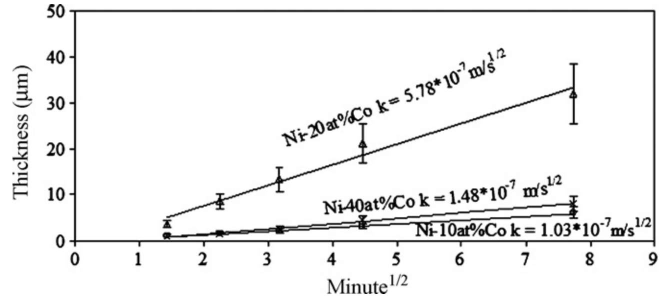

Fig. 7. Total thickness of the reaction phases as a function of the reaction time.

growth rate constants of the three reaction couples are 1.03×10^{-7}, 5.78×10^{-7}, and 1.48×10^{-7} m/s$^{1/2}$, respectively. The Ni–10 at%Co substrate has the lowest reaction rate, and Ni–20 at%Co substrate has the highest reaction rate.

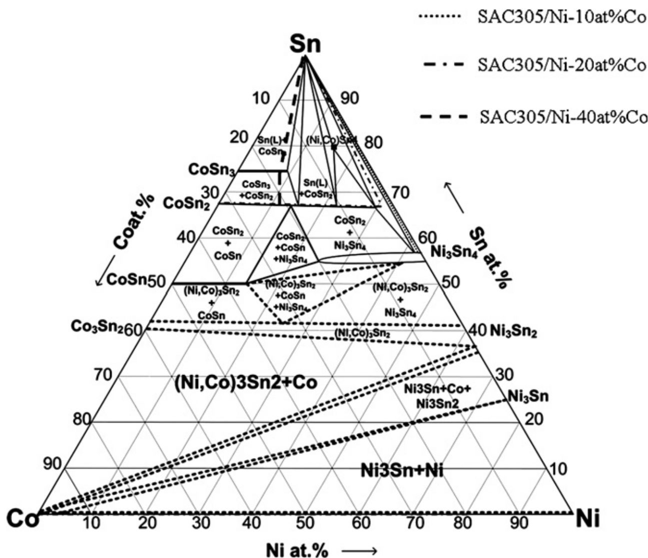

Fig. 6. Sn–Ni–Co isothermal section superimposed with the reaction paths of SAC305/Ni–Co couples reacted at 250 °C.

4. Conclusion

The wetting properties of Ni–Co alloys by the SAC305 solder are better than the currently used Ni–7 wt%V alloy. With increased Co additions, the surface roughness increase, and the wetting properties decrease. SAC305/Ni–Co interfacial reactions depend on Co additions. When Co increases to 10 at%, the Co effect is smaller than that of Cu, and the SAC305/Ni–10 at%Co interfacial reaction is similar to SAC305/Ni. When Co increases to 20 at%, the Co effect is comparable to that of Cu, and forms the Ni_3Sn_4 and $CoSn_2$ phases. When Co increases to 40 at%, Co dominates the interfacial reactions, forming the $CoSn_2$ and α-$CoSn_3$ phases. As the Co addition increases, the reaction path shifts from the Sn–Ni side towards the Sn–Co side. Ag remains inactive. The Ni–10 at%Co

substrate has the lowest reaction rate among the three different Ni–Co alloys.

Acknowledgement

The authors acknowledge the Center-of-Excellence (COE) Program on Membrane Technology from the Ministry of Education, Taiwan, the Distinctive Research Area project of the Chung Yuan Christian University, Taiwan (Grant # CYCU-98-CR-CE), and the National Science Council (Grant # NSC98–2221-E-033-074) for their financial support.

References

[1] K. Yamanaka, Y. Tsukada, K. Suganuma, J. Alloy Compd. 437 (1–2) (2007) 186–190.
[2] C.-M. Chen, K.-J. Wang, K.-C. Chen, J. Alloy Compd. 432 (1–2) (2007) 122–128.
[3] C.-C. Chen, S.-W. Chen, C.-H. Chang, J. Mater. Res. 23 (7) (2008) 1895–1901.
[4] C.-C. Chen, S.-W. Chen, C.-H. Chang, J. Mater. Res. 23 (10) (2008) 2743–2748.
[5] Y.-C. Lin, J.-G. Duh, B.-S. Chiou, J. Electron. Mater. 35 (1) (2006) 7–14.
[6] B.-L. Young, J.-G. Duh, B.-S. Chiou, J. Electron. Mater. 30 (5) (2001) 543–553.
[7] H. Han, Y.C. Sohn, J. Yu, J. Electron. Mater. 36 (5) (2007) 578–586.
[8] A. Kumar, M. Kumar, D. Kumar, Microelectron. Eng. 87 (2010) 387–390.
[9] R. Labie, E. Beyne, P. Ratchev, Proceedings of the 53th Electronic Components & Technology Conference, 2003, pp. 1230–1234.
[10] C.-C. Chen, Y.-T. Chan, Intermetallics 18 (4) (2010) 649–654.
[11] R. Labie, P. Ratchev, E. Beyne, Proceedings of the 55th Electronic Components & Technology Conference, vol. 1, 2005, pp. 449–451.
[12] W.J. Zhu, J. Wang, H.S. Liu, Z.P. Jin, W.P. Gong, Mater. Sci. Eng. A 456 (2007) 109–113.
[13] W.-C. Wu, T.-E. Hsieh, H.-C. Pan, J. Electrochem. Soc. 155 (5) (2008) D369–376.
[14] W.C. Luo, C.E. Ho, J.Y. Tsai, Y.L. Lin, C.R. Kao, Mater. Sci. Eng. A 396 (2005) 385–391.
[15] H.-S. Chun, J.-W. Yoon, S.-B. Jung, J. Alloy Compd. 439 (1–2) (2007) 91–96.
[16] K.S. Kim, S.H. Huh, K. Suganuma, J. Alloy Compd. 352 (2003) 226–236.
[17] H.-J. Lin, J.-S. Lin, T.-H. Chuang, J. Alloy Compd. 487 (1–2) (2009) 458–465.
[18] J.-W. Yoona, B.-I. Noha, B.-K. Kimb, C.-C. Shura, S.-B. Jung, J. Alloy Compd. 486 (1–2) (2009) 142–147.
[19] H.K. Kim, H.K. Liou, K.N. Tu, J. Mater. Res. 10 (3) (1995) 497–504.
[20] Y.-Y. Chen, J.-G. Duh, B.-S. Chiou, J. Mater. Sci.: Mater. Electron. 11 (2000) 279–283.
[21] C.Y. Liu, J. Li, G.J. Vandentop, W.J. Choi, K.N. Tu, J. Electron. Mater. 30 (5) (2001) 521–525.
[22] J.-I. Lee, S.-W. Chen, H.-Y. Chang, C.-M. Chen, J. Electron. Mater. 32 (3) (2003) 117–122.
[23] H.-Y. Chang, S.-W. Chen, D.S.-H. Wong, H.-F. Hsu, J. Mater. Res. 18 (6) (2003) 1420–1428.
[24] M.G. Cho, S.-K. Seo, H.M. Lee, J. Alloy Compd. 474 (1–2) (2009) 510–516.
[25] E. Saiz, C.-W. Hwang, K. Suganuma, A.P. Tomsia, Acta Mater. 51 (11) (2003) 3185–3197.
[26] T. Matsumoto, K. Nogi, Ann. Rev. Mater. Res. 38 (2008) 251–273.
[27] S. Amore, E. Ricci, G. Borzone, R. Novakovic, Mater. Sci. Eng. A 495 (1–2) (2008) 108–112.
[28] L. Zang, Z. Yuan, H. Zhao, X. Zhang, Mater. Lett. 63 (23) (2009) 2067–2069.
[29] K.Y. Hwan, H.H. Kwan, J. Alloy Compd 477 (1–2) (2009) 278–282.
[30] I. Jung, M.G. Cho, H.M. Lee, J. Electron. Mater. 38 (11) (2009) 2301–2307.
[31] S.C. Yang, W.C. Chang, Y.W. Wang, C.R. Kao, J. Electron. Mater. 38 (1) (2009) 25–32.
[32] F.G. Yost, F.M. Hosking, D.R. Frear, The Mechanics of Solder Alloy Wetting and Spreading, Van Nostrand Reinhold, New York, 1993.
[33] R. Shuttleworth, G.L.J. Bailey, Discuss. Faraday Soc. 3 (1948) 16–22.
[34] T. Nishizawa, K. Ishida, in: T.B. Massalski (Ed.), Binary Alloy Phase Diagrams, ASM, Materials Park, OH, 1990, pp. 1214–1215.
[35] D.J. Chakrabarti, D.E. Laughlin, S.-W. Chen, Y.A. Chang, in: P. Nash (Ed.), Phase Diagrams of Binary Nickel Alloys, ASM, Materials Park, OH, 1990, pp. 85–95.
[36] C.-H. Lin, S.-W. Chen, C.-H. Wang, J. Electron. Mater. 31 (9) (2002) 907–915.
[37] C.-H. Wang, S.-W. Chen, Metall. Mater. Trans. A 34 (2003) 2281–2287.
[38] Y.-H. Chao, S.-W. Chen, C.-H. Chang, C.-C. Chen, Metall. Mater. Trans. A 39 (3) (2008) 477–489.
[39] P. Nash, A. Nash, Bull. Alloy Phase Diagram 6 (4) (1985) 350–359.
[40] C. Schmetterer, H. Flandorfer, K.W. Richter, U. Saeed, M. Kauffman, P. Roussel, H. Ipser, Intermetallics 15 (2007) 869–884.
[41] A. Lang, W. Jeitschko, Z. Metallkd. 87 (1996) 759–764.
[42] Y. Takashi, S. Shigeaki, K. Shinji, U. Keisuke, K. Kojiro, I. Masaaki, S. Kazuhiro, H. Akio, Y. Masaharu, Mater. Trans. 46 (2005) 2406–2412.
[43] C.-W. Chen, Interfacial reaction between Sn(Cu) solder and NiCo alloy UBM, Master Thesis, National Center University, Taiwan, 2009.
[44] S.-W. Chen, C.-H. Wang, J. Mater. Res. 21 (9) (2006) 2270–2277.
[45] H. Nishikawa, A. Komatsu, T. Takemoto, Mater. Trans. 46 (11) (2005) 2394–2399.
[46] C.-C. Chen, W. Gierlotka, S.-W. Chen, J. Electron. Mater. 37 (2008) 1727–1733.
[47] F.J.J. van Loo, G.D. Rieck, Acta Metall. 21 (1973) 61–71.
[48] V.I. Dybkov, Reaction Diffusion and Solid State Chemical Kinetics, IPMS Publications, 2002.